Published in final edited form as:

Nat Biomed Eng. 2020 March ; 4(3): 335–342. doi:10.1038/s41551-019-0499-8.

^{1}H magnetic resonance spectroscopy of ^{2}H-to-^{1}H exchange quantifies the dynamics of cellular metabolism in vivo

Laurie J Rich[1,&], **Puneet Bagga**[1,&], **Neil E. Wilson**[1], **Mitchell D Schnall**[1], **John A Detre**[1,2], **Mohammad Haris**[1,3,4], **Ravinder Reddy**[1,*]

[1]Center for Magnetic Resonance and Optical Imaging, Department of Radiology, Perelman School of Medicine at the University of Pennsylvania, Philadelphia, PA, USA

[2]Department of Neurology, Perelman School of Medicine at the University of Pennsylvania, Philadelphia, PA, USA

[3]Research Branch, Sidra Medicine, Doha, Qatar

[4]Laboratory Animal Research Center, Qatar University, Doha, Qatar

Abstract

The quantitative mapping of the in vivo dynamics of cellular metabolism via non-invasive imaging contributes to the understanding of the initiation and progression of diseases associated with dysregulated metabolic processes. Current methods for imaging cellular metabolism are limited by low sensitivities, by costs, or by the use of specialized hardware. Here, we introduce a method that captures the turnover of cellular metabolites by quantifying signal reductions in proton magnetic resonance spectroscopy (MRS) resulting from the replacement of ^{1}H with ^{2}H. The method, which we termed quantitative exchanged-label turnover MRS, only requires deuterium-labelled glucose and standard MRI scanners, and with a single acquisition provides steady-state information and metabolic rates for several metabolites. We used the method to monitor glutamate, glutamine, γ-aminobutyric acid and lactate in the brains of normal and glioma-bearing rats following the administration of $^{2}H_2$-labelled glucose and $^{2}H_3$-labelled acetate. Quantitative exchanged-label turnover MRS should broaden the applications of routine ^{1}H MRS.

Cellular metabolism is maintained by a network of biochemical reactions essential for normal tissue function[1]. These reactions form larger metabolic pathways which exist under tight regulatory control to help balance metabolic fluctuations experienced by the cell.

*Corresponding author, krr@pennmedicine.upenn.edu.

Author contributions

RR provided overall experimental design, conception and contributed to data analyses, manuscript writing and editing. LR, PB contributed to conception and design of the study, performed experiments, analyzed data and wrote the manuscript. NW provided insights on data analyses and contributed to spectral denoising of datasets. MDS, JAD, MH contributed to manuscript writing and editing.

&These authors contributed equally

Competing interests

The authors declare no competing interests.

Therefore, it is not surprising that abnormal metabolism is a hallmark of several pathologies including neurodegeneration and cancer[1,2]. Probing the kinetics of metabolic pathways *in vivo* plays a key role in studying disease mechanisms, identifying new treatment strategies, and developing biomarkers of treatment response. To date, several non-invasive techniques have been established to monitor the relationship between cellular function and metabolism[3].

Positron emission tomography (PET) using the glucose analog 2-^{18}F-fluoro-2-deoxy-d-glucose (^{18}FDG) is a widely utilized clinical tool that provides high-resolution maps of glucose uptake in cancer, neurodegeneration, and cardiac diseases[4–6]. However, PET also requires the use of radioactive ^{18}FDG and does not readily provide information on tissue metabolic activity beyond the initial step of glycolytic metabolism[7]. Conventional magnetic resonance imaging (MRI) provides outstanding anatomical information without exposure to ionizing radiation, but only offers limited insight in regards to metabolism[8]. Chemical exchange saturation transfer (CEST) MRI offers enhanced detection sensitivity for a variety of metabolites, but is limited in its ability to measure dynamic changes in metabolite turnover[9,10]. Proton magnetic resonance spectroscopy (^{1}H MRS) is a gold standard for detecting and quantifying several endogenous tissue metabolites in a single acquisition, but is not capable of tracking metabolic fluxes and pathways[11]. ^{13}C MRS in combination with administration of ^{13}C-labelled substrates has been used to study metabolic pathways in both preclinical and clinical settings[12–14], but its low sensitivity has limited its routine use in human studies. The advent of dynamic nuclear polarization combined with ^{13}C MRS has provided a strong boost to the sensitivity of this technique[15,16]. However, this approach is hindered by the short *in vivo* half-life of hyperpolarized ^{13}C in addition to the requirement of onsite polarizers and ^{13}C-hardware.

Recently, ^{2}H MRS, also referred to as deuterium MRS (DMRS), has been evaluated for its potential to assess tissue metabolic kinetics following administration of deuterated subtrates[17]. Preliminary studies have demonstrated the utility of DMRS based deuterium metabolic imaging (DMI) in detection of human glioblastoma and hepatocellular carcinomas[18]. However, DMRS has low sensitivity relative to ^{1}H MRS and still requires specialized hardware for use on clinical scanners. Deuterated substrates have also been utilized in combination with stimulated Raman-scattering imaging for spectral tracing of deuterium (STRIDE) to measure metabolic dynamics of newly synthesized cellular macromolecules including DNA, proteins, lipids and glycogen[19]. Although this approach provides high-resolution, biochemically informative images on glucose anabolic utilization, it is mostly restricted to superficial tissue measurements and requires prolonged exposure (~10 days) to deuterated substrates.

Here we present a method, **q**uantitative **e**xchanged-**l**abel **t**urnover (QELT) MRS, or simply qMRS, that increases the sensitivity of magnetic resonance based metabolic mapping without the requirement for specialized hardware. Similar to DMRS, qMRS relies on the administration of deuterium labelled substrates to track production of downstream metabolites. However, instead of ^{2}H based detection of these metabolites, we performed ^{1}H MRS. Since ^{2}H is invisible on ^{1}H MRS, replacement of ^{1}H with ^{2}H leads to an overall reduction in ^{1}H MRS signal for the corresponding metabolites. This method takes advantage

of the universal availability and ease of implementation of ^{1}H MRS on all clinical and preclinical MR scanners. The exceptional spectral resolution offered by ^{1}H MRS enables tracking of label transfer to several important metabolites, including glutamate (Glu), glutamine (Gln), γ-aminobutyric acid (GABA), and lactate (Lac). Proof of principle qMRS studies were performed in the brains of normal and glioma bearing rats following the administration of [6,6′−$^{2}H_2$]glucose and [2,2,2′−$^{2}H_3$]acetate. Together, our findings highlight qMRS as a straightforward and promising strategy for monitoring cellular metabolism *in vivo* with a high potential for widespread clinical translation.

Results

Fundamentals of qMRS: Pilot Study

Administration of labelled substrates such as glucose or acetate can provide information on metabolic flux through glycolysis and the citric acid cycle by tracking downstream labelling of metabolites including Glu, Gln, GABA and Lac (Fig. 1a)[20,21]. Building on the recent advances of DMRS, we developed qMRS which relies on the indirect detection of transferred deuterium label from deuterated substrates to intermediate metabolites. As a proof of concept, we performed qMRS in the brain of healthy rats before and after administration of [6,6′−$^{2}H_2$]glucose. Figure 1b shows localized ^{1}H MRS spectra from a rat brain before and post 60 minutes of [6,6′−$^{2}H_2$]glucose infusion. Post infusion, a reduction in the Glu-H4 amplitude at 2.35 ppm can be clearly observed. Similar observations were also made following infusion of [2,2,2′−$^{2}H_3$]acetate (Fig. S1). Subtraction of the post-infusion ^{1}H MRS spectrum from the pre-infusion spectra revealed a marked increase in the 2.35 ppm Glu-H4 resonance, in addition to several Glu, Gln, GABA and aspartate (Asp) resonances, all of which were well above background signal. A large reduction in the difference spectrum was also observed between 3.3–3.6 ppm associated with non-deuterated proton resonances on the infused [6,6′−$^{2}H_2$]glucose (Fig. 1B **right**). In contrast, a considerable increase can be observed between 3.6–4.0 ppm corresponding to the deuterium labelled glucose-H6 resonance (3.9 ppm) and Glx-H2 (3.8 ppm). A slight decrease was also observed at the 1.33 ppm Lac-H3 resonance, which is likely related to small amounts of unlabelled Lac produced by cerebral due to glucose infusion[18]. This proof-of-principal study highlights the potential of qMRS to track ^{2}H based labelling of metabolites with high sensitivity, all of which can be simply performed with a traditional ^{1}H MRS approach.

Comparative detection of neural metabolite turnover with qMRS and DMRS

Previous work has demonstrated the ability of DMRS to track the production of Glx and lactate following [6,6′−$^{2}H_2$]glucose infusion with high temporal resolution[17]. Therefore, we tested whether qMRS could also provide similar information following [6,6′−$^{2}H_2$]glucose administration. To test this, we compared Glx measurements in healthy rat brain (n=4) made with qMRS and DMRS using a combined ^{1}H volume coil and ^{2}H surface coil setup (Fig. S2), with acquisition of qMRS and DMRS spectra alternating every five minutes following infusion. Figure 2 compares the time courses of qMRS and DMRS spectra pre- and post-infusion of [6,6′−$^{2}H_2$]labelled glucose. Infusion of [6,6′−$^{2}H_2$]glucose revealed a visible reduction in the 2.35 ppm Glu-H4 peak after only 20 mins of infusion, with the largest reduction observed at 60 mins (Fig. 2a). The qMRS difference spectra confirmed this, with

clear labelling of the Glu-H4 and other Glx resonances beginning after 20 mins of infusion (Fig. 2b). Similarly, the formation of a Glx peak in DMRS was clearly observed within 20 mins during infusion and continued to increase steadily over time (Fig. 2c). Surprisingly, a lactate peak was observed after 60 minutes of infusion using DMRS, which was not detected with qMRS. One explanation is that for DMRS studies, a surface coil with an unlocalized pulse-acquire sequence was utilized. Therefore, the signal measured with this approach could be from tissues other than the brain where labelled lactate is generated. In contrast, we performed localized spectroscopy for qMRS, where, as previously demonstrated[18], we do not expect any lactate labelling in the healthy brain.

Following acquisition of combined qMRS and DMRS data sets, Glx concentrations were quantified using LCModel[22] (qMRS) and AMARES[23] (DMRS) for each timepoint. Comparison of Glx measurements were in good agreement, with an initial linear increase that began to plateau after 45 mins of infusion for both qMRS and DMRS (Fig. 3a). Furthermore, correlation analysis revealed a positive correlation ($R^2 = 0.38$) between these measurements, indicating that qMRS accurately reflects the dynamic labelling of Glx following deuterated glucose administration (Fig. 3b). This was confirmed using a Bland-Altman analysis, which revealed minimal bias between the Glx measurements obtained with qMRS and DMRS (Fig. 3c). In addition to Glx estimates, we compared SNR levels measured for the Glx peak obtained with our qMRS and DMRS setup. We calculated SNR to be ~41 for qMRS and ~8 for DMRS prior to subtraction, and ~8 and ~5 for the corresponding differences estimated for each spectrum. This represents an almost 5-fold higher sensitivity for qMRS over DMRS, and 60% higher sensitivity for the corresponding difference spectra. Since DMRS was obtained with a surface coil with a pulse-acquire acquisition, while qMRS was obtained with a volume coil with Point RESolved Spectroscopy (PRESS) localization, the SNR advantages described for qMRS is still somewhat underestimated due to the coil sensitivity differences and longer echo times involved in the spatial localization.

Tracking of 2H labelling of neural metabolites with qMRS

While DMRS can provide temporal information on metabolite labelling, it is primarily restricted to Glx and Lac quantification due to the broad spectral peaks obtained through ^2H detection. In contrast, since qMRS measures changes in the ^1H MRS spectra, the high spectral resolution should enable detection of several key neural metabolites not obtainable with DMRS. For instance, instead of a single Glx peak, qMRS allows for individual detection of Glu and Gln, both of which are important components of neural metabolism and signaling. Therefore, we next set to measure labelling of these metabolites post [6,6′ $-^2H_2$]glucose infusion. To quantify labelling, qMRS with [6,6′$-^2H_2$]glucose infusion was performed in the brain of healthy rats (n=6) over a 45 minute period. All ^1H MRS spectra were analyzed with LCModel to obtain metabolite concentrations before and after infusion. To estimate the degree of labelling for each metabolite, post-infusion concentration measurements for each timepoint were subtracted from pre-infusion measurements, and divided by pre-infusion values to obtain the percentage of fractional enrichment. These values were adjusted by a correction factor of 1.33 to adjust for the theoretical probability

that either a single or two ^{2}H groups will be transferred from acetyl-coA to downstream metabolites after [6,6′−$^{2}H_2$]glucose infusion.

Quantification of the Glx fractional enrichment (Fig. 4a) revealed a gradual increase and eventual plateau during infusion, with a 0.89 ± 0.23 mM increase (~9% enrichment) at 45 min post infusion. Importantly, qMRS enabled individual quantification of changes in Glu (Fig. 4B) and Gln (Fig. 4C) levels, with an 0.68 ± 0.15 mM (~11% enrichment) increase in Glu and 0.21 ± 0.12 mM (8% enrichment) increase in Gln observed 45 min post [6,6′−$^{2}H_2$]glucose infusion. It was also possible to estimate changes in GABA (Fig. 4D) concentration, with a 0.25 ± 0.10 mM increase (10% enrichment) after infusion. Visually, the fractional enrichment of most metabolites followed an exponential pattern of increase over time. These labelling patterns are similar in regards to fractional enrichment of metabolites with published ^{13}C MRS literature[21,24]. Changes in these metabolites were also compared with N-acetyl aspartate (NAA), a highly abundant amino acid in the brain[25], as it should remain unlabelled throughout the experiment. As expected, NAA levels (Fig. 4e) did not vary considerably throughout the experiment, suggesting it is a suitable reference for qMRS studies in the brain. In addition to [6,6′−$^{2}H_2$]glucose, infusion of unlabelled glucose was performed in a subset of animals (n=4) to determine the stability of qMRS measurements over time. We did not observe significant changes in the metabolite concentrations following the infusion of unlabelled glucose (Fig. S3). Quantification of Glu and Gln was also possible following infusion of [2,2,2′−$^{2}H_3$]acetate (Fig. S4). These results clearly demonstrate the ability of qMRS for measuring individual Glu and Gln metabolite labelling.

qMRS enables detection of glycolytic metabolism in glioblastoma

It is well recognized that brain tumour development is associated with significant changes in cellular metabolism[2]. In particular, tumour cells are known to rely more heavily on glycolysis over oxidative phosphorylation to support cell growth, proliferation and survival[26]. A hallmark of this inefficient metabolic process is the increased uptake of glucose and subsequent conversion to lactate, with lactate production increasing significantly compared to normal physiological conditions. Given this, we hypothesized that qMRS should be capable of capturing this increased lactate turnover in brain malignancies. To address this, rats (n=3) were orthotopically implanted with the F98 syngeneic rat glioma model and allowed to grow for three weeks, after which qMRS was performed. Figure 5 displays representative qMRS spectra from an F98 glioblastoma bearing rat acquired before and 60 mins after [6,6′−$^{2}H_2$]glucose infusion. Prior to infusion, a large peak can be observed at 1.33 ppm representing combined lactate and lipid peaks (Fig. 5a). After 60 min of [6,6′−$^{2}H_2$]glucose infusion, a marked reduction in the Lac-H3 peak at 1.33 ppm was observed suggesting considerable ^{2}H labelling of lactate (Fig. 5b). This was in contrast to non-tumour bearing animals where no significant change in the Lac peak was observed. Subtraction of post-infusion ^{1}H MRS spectra from the pre-infusion spectra show the time course of lactate labelling over the entire 60 min period, with a clear increase in labelling occurring only 10 min post-infusion (Fig. 5c). These results are consistent with previously published results using DMRS following the infusion of [6,6′−$^{2}H_2$]glucose[18].

In vivo mapping of cerebral metabolism

Finally, to expand our observations beyond a basic single voxel acquisition, we performed spectroscopic imaging to map deuterium labelling of metabolites occurring throughout the brain. To accomplish this, Chemical shift imaging (CSI) was performed in a healthy rat brain before and 60 min post infusion of [6,6′−$^2H_2$]glucose. A CSI volume of interest (VOI) was positioned over the center of the brain (Fig. 6a **left**). Metabolite maps were generated by calculating Glu and NAA concentrations for each voxel using LCModel, creating colourmaps based on these estimates and overlaying these maps on an anatomical image. Before infusion, Glu and NAA maps revealed a range of metabolite levels across the imaging area (Fig. 6a **right**). After [6,6′−$^2H_2$]glucose infusion, a clear reduction in Glu levels can be observed for the entire region, whereas NAA levels remained relatively constant. We then compared spectra obtained from a single CSI voxel within the VOI. Comparison of the spectra confirmed these findings, with a marked reduction in the Glu-H4 amplitude detected post infusion and a clear peak formed at 2.35 ppm in the difference spectra (Fig. 6b). Spectra obtained for several of the acquired CSI voxels also confirmed these observations (Fig. S5). Together, these findings demonstrate the feasibility of performing ^1H based spectroscopic imaging in conjunction with deuterium labelling, and support continued development of qMRS for human studies.

Discussion

We report a promising approach (qMRS) to measure the exchange of deuterium label from metabolic substrates to metabolic intermediates in normal rat brain and rat glioblastoma using a common and easily implementable ^1H MRS technique. qMRS not only provides a sensitivity advantage compared to DMRS, but it can also be carried out using standard clinical MRI hardware. Given ongoing efforts to establish robust acquisition and analysis methodologies for clinical ^1H MRS[27], we expect that qMRS will be easily implemented on 3T and 7T clinical scanners, making it relatively straight-forward to translate to clinical use. It is also possible to further improve qMRS by applying spectral denoising strategies[28–30] (Fig. S6). For instance, singular value decomposition noise reduction has been recently applied in ^{13}C MRS analysis to enable differentiation of true from false peaks in noisy datasets[30]. Integration of these approaches with qMRS could therefore enable measurement of tissue metabolic kinetics with high temporal resolution by reducing the number of averages necessary for spectral analysis.

Although only qMRS and DMRS were compared in this work, deuterated substrates have also been applied for stimulated Raman-scattering based imaging of cellular metabolism. Using the STRIDE approach, previous studies[19] were able to produce high resolution images of deuterium labelled macromolecule metabolites (DNA, lipids, proteins) following administration of deuterium labelled glucose. While this technique was performed in a variety of tissues including brain, intestine, liver and tumours, it is restricted to superficial imaging depths and therefore its clinical potential is limited. Furthermore, in contrast to qMRS and DMRS, this approach requires prolonged administration of labelled glucose and has a 10 mM detection limit which is considerably higher than qMRS (~0.5 mM). A major benefit of the qMRS approach compared to the recently developed DMRS is that it is

feasible to measure deuterium labelling for individual metabolites such as Gln, Glu, GABA and Lac. Dynamic exchange of label on these metabolites as a function of time following the infusion of deuterium labelled glucose (or acetate) can be used to derive rates of glycolysis, oxidative phosphorylation (OXPHOS) and glutamate/GABA-glutamine cycling *in vivo* in a spatially dependent manner[31]. This information can be particularly useful when studying metabolic derangements in disease. For instance, glutamate/GABA-glutamine cycling exists in a careful balance within the healthy human brain to maintain normal neurotransmission. However, changes in this cycling are associated with severe neurological disorders such as Alzheimer's and epilepsy[32,33]. In addition, as observed in our rat glioblastoma studies, a hallmark of many cancers increase lactate production due to a metabolic switch from OXPHOS to glycolysis to support tumour growth[26]. Detection and quantification of the rate of lactate production may provide crucial information regarding tumour metabolism. Hence, qMRS is expected to open up new opportunities to probe changes in these metabolic rates in a variety of human diseases, including cancer and neurological disorders.

Although technically and experimentally challenging, over the last 3 decades ^{13}C MRS is universally accepted as the only non-invasive method for providing information on the relationship between neuroenergetics and neuronal function[34,35]. The time course of the incorporation of ^{13}C label from ^{13}C-labelled glucose into Glu-C4 and Gln-C4 resonances (fractional enrichment, FE) is used in all studies to provide quantitative information regarding the rates of glutamatergic TCA cycle and neurotransmission[17,36]. Similar to ^{13}C studies, we observed the exponential pattern of ^{2}H labelling of Glu and Gln resonances using qMRS in the rat brain. We have not quantified the metabolic fluxes by fitting the FE data obtained via qMRS experiments in the present study, nonetheless, we anticipate that these results would compare well with the values already reported in the literature[17,37,38].

qMRS offers several advantages over existing methods for measuring *in vivo* metabolism. Most notably, it only requires deuterium labelled glucose, which can be given as an oral drink[18], along with standard 3T MRI scanners (or 7T MRI). There is no risk of exposure to ionizing radiation, and no special equipment such as onsite hyperpolarizers for ^{13}C, multinuclear coils or cyclotrons for PET are needed. The deuterium labelled turnover is monitored directly using standard ^{1}H MRS acquisition hardware and signal processing strategies. Given this, the overall experimental simplicity and cost per scan makes qMRS an ideal choice for studying *in vivo* metabolic processes in the research and clinical setting. Another major advantage of qMRS is that it provides steady state metabolic information of several metabolites along with the labelling kinetics of key metabolites in the same acquisition. Therefore, it is possible to obtain information on both labelled and unlabelled metabolites. While this method is demonstrated using glucose and acetate, it is also applicable to measure label exchange from other deuterated substrates with their corresponding unlabelled metabolites. Moreover, this general approach is equally applicable to studying ^{19}F-labelled substrates to probe metabolism and metabolite pool size changes. Finally, we showed that it is possible to extend this approach to spectroscopic imaging modes allowing labelling studies that can be performed across entire tissues with high sensitivity. Therefore, we anticipate qMRS can also be implemented in other organ systems including liver, heart and breast.

Despite the advantages, the approach has some limitations. Since ^{1}H MRS is sensitive to motion, repeated movements can lead to changes in peak linewidth, frequency shifts, and even peak area[39]. Therefore, subtraction of spectra acquired over time can be challenging. One approach to overcome motion related frequency shifts is to perform block averaging using a small number of acquisitions (4 or 8), and perform a Fourier transform and frequency alignment using either NAA or Cr peaks as a chemical shift reference. This can also be combined with advanced quantification methods such as LCModel to improve the accuracy of metabolite turnover quantification. Furthermore, ^{1}H MRS is also susceptible to background signals that will be augmented in cases where lipid signals are high (e.g. tumours, breast, skeletal muscle etc.). However, strategies such as variable echo time[40] and/or multi-quantum filtering[41] could be applied to mitigate these issues. However, strategies such as variable echo time[40] and/or multi-quantum filtering[41] could be applied to mitigate these issues. It is also important to note that while LCModel was used for quantification of metabolite labelling in this study, it is unclear how deuterium labelling patterns may affect the accuracy of these measurements. For instance, the average number of deuterons at the C4 position of Glu after [6,6′–$^{2}H_2$]glucose infusion is always lower than two because of ^{2}H label loss in the TCA cycle at the conversion of acetyl-CoA to citrate. As described previously[18], the theoretical chance that both deuterons or only a single ^{2}H atom is transferred from acetyl-CoA to Glx will be 1.33. Although we normalized the individual concentrations of metabolites obtained in the current study, further consideration is necessary to derive correction factors for all metabolites measured with qMRS. It is also likely that J-coupling patterns for specific metabolites may be altered following deuterium labelling and that certain proton resonances will be labelled at greater frequencies than others. Ideally, individual basis sets should be created which mimic expected labelling patterns in vivo, but this becomes increasingly difficult as these patterns change dynamically over time. Although this did not seem to negatively impact our analysis, optimizing these analysis parameters and/or determining the most suitable analysis method is a logical direction for future qMRS studies.

Outlook

In summary, we demonstrated a technique that has the potential to measure glycolytic metabolism, OXPHOS, and glutamate-glutamine cycling in normal brain and tumours via the utilization of deuterium labelled substrates (glucose and acetate) and ^{1}H MRS. Deuterated substrates can be safely and easily administered to humans at low doses[18]. While the studies described here were preclinical in nature, we expect that this method can be easily extended to human studies at 3T and 7T, where CSI is routinely performed in research. As such, current efforts in our group are focused on developing qMRS for use in human subjects. This approach is expected to enable a wide range of studies probing metabolic derangements in vivo across medical disciplines.

Methods

Animal models and preparation

All the animal experiments were performed under an approved IACUC protocol by the University of Pennsylvania. For qMRS metabolite tracking studies, seven 13–15 week old male Fischer CDF rats (220–250 g, Charles River, Wilmington, MA) were used. Four of the male CDF rats were then chosen for a second imaging session to perform dual qMRS and DMRS. For brain tumour studies, three 6–8 week old female F344/NCR rats (120–130 g, Charles River, Wilmington, MA) were implanted with the rat glioblastoma cell line (F98)[42] as described previously[43]. Briefly, general anesthesia was induced using 2% isoflurane mixed with 1 liter/min oxygen followed by 1–2% isoflurane. The animal head was fixed on a stereotactic apparatus while anesthetized. Following an incision made on the skin covering the skull, a hole was drilled at 3 mm lateral and 3 mm posterior to the bregma. A 10 μl suspension of 5×10^5 F98 cells (ATCC®, Manassas, VA) in PBS was injected (500 nl/min) into the cortex at a depth of 2.5 mm with a Hamilton syringe and a 30-gauge needle using stereotactic apparatus. Three weeks post implantation of F98 cells, the rats were subjected to MRS.

MR studies and metabolite quantification

All the preclinical MRI and MRS experiments were performed on a 9.4T, 30 cm horizontal bore magnet interfaced to a Bruker console (Paravision 6.0.1) using both custom built and commercial radiofrequency (RF) coils. Animals were anesthetized using 1.5–2% isoflurane mixed with air at 1 L/min, and secured to a body-bed inside a 35-mm diameter volume coil (M2M Imaging Corp., Cleveland, OH). In dual $^1H/^2H$ MRS studies, a custom-built deuterium single loop RF coil was positioned on the head of the rats within the proton volume coil. This RF coil assembly allowed us to perform alternating qMRS and DMRS acquisitions (Fig. S2). Body temperature was monitored using a rectal temperature probe and maintained at 37 °C using warm air blown inside the bore of the magnet. Rats were injected with [6,6′−$^2H_2$]glucose (Cambridge Isotope Laboratories Inc, Tewksbury, MA) at a dose of 1.95 g/kg for a period up to 70 mins via an automated infusion pump and tail vein catheter using a bolus variable infusion protocol as described previously[44,45]. Briefly, animals received a 250 μL bolus of [6,6′−$^2H_2$]glucose by intravenous infusion over a 15 sec period. The infusion rate was then reduced to 191 μL/min and decreased manually every 30 s following a decreasing exponential function to a final infusion rate of 13.7 μL/min during the first 8 min. After this period, the infusion rate remained constant for the remainder of the experiment. The maximum infusion volume over the imaging period was 1.5 mL.

qMRS spectra were acquired from a voxel localized in the mid-brain ($6.5\times6.5\times2.5$ mm^3) in both control (n = 6) and glioblastoma ($4\times4\times4$ mm^3) bearing (n = 3) rats using PRESS[46] (TR/TE=2500/16 ms, spectral width = 4 kHz, 90° pulse bandwidth = 5400 Hz, 180° pulse bandwidth = 2400 Hz, number of points = 4006, variable power RF pulses with optimized relaxation delays (VAPOR)[47] water suppression, averages=128). An additional qMRS dataset (n=1) was acquired in a control rat with a larger number of averages (256 averages, 10 min acquisition) to obtain representative difference spectra to show metabolite labelling in Figure 1 and 2. DMRS spectra were acquired using a non-localized pulse-acquire

sequence for the entire volume of the surface coil (TR = 300 ms, flip angle = 20°, number of averages = 1000). The acquisition parameters were empirically optimized by adjusting flip angle and TR to obtain high SNR, however further optimization to improve SNR in future studies is warranted. For CSI datasets, a PRESS based pulse sequence was used with the following parameters: TR/TE = 1500/16 ms, slice thickness = 3 mm, total FOV = 35 × 35 mm, excited FOV = 10 × 6.5 mm, matrix size = 12 × 12, number of points = 1024, spectral width = 10000 Hz, 90° pulse bandwidth = 8000 Hz, 180° pulse bandwidth = 8000 Hz, VAPOR water suppression, scan time = 20 min. In addition to water suppressed spectrum, another spectrum was acquired without water suppression to obtain the water reference signal for normalization. In combined qMRS/DMRS quantification studies, spectra were acquired every other 5 minutes giving 10 minute temporal resolution for each nuclei. All displayed spectra were processed using the Bruker TOPSPIN software package (Version 4.0.6).

Quantification

Metabolite concentrations measured by *in vivo* ^{1}H MRS were quantified using LCModel software (Version 6.3), a widely applied MRS analysis tool which employs a least-squares based prior-knowledge fitting program[22]. The concentration of metabolites was measured using the unsuppressed water peak as a concentration standard. LCModel applied a 9.4T spin echo (TE=16 ms) basis set incorporating the following resonances: alanine (Ala), aspartate (Asp), creatine (Cr), phosphocreatine (PCr), gamma-aminobutyric acid (GABA), glucose (Glc), glutamine (Gln), glutamate (Glu), glycerophosphocholine (GPC), phosphocholine (PCh), glutathione (GSH), myo-inositol (Ins), N-acetyl aspartate (NAA), N-acetyl aspartate+glutamate (NAAG), sycllo-inositol, taurine (Tau), lipid resonances at 0.9, 1.3 and 2.0 ppm and macromolecule resonances at 0.9, 1.2, 1.4, 1.7 and 2.0 ppm. Once each metabolite concentration was estimated, calculation of fractional enrichment for each metabolite was performed by subtracting post-infusion levels from pre-infusion levels and dividing this value from pre-infusion levels. SNR estimates were calculated using Bruker topspin software by taking the ratio of the peak area divided by the standard deviation of the noise in the spectrum.

Analysis of CSI datasets was performed by calculating Glu and NAA concentrations for each voxel within the VOI using LCModel. LCModel based metabolite concentration estimates were loaded into MATLAB (R2018a) as a 2D matrix and filtered using 2D gaussian smoothing. The 3×3 matrix was interpolated to a 9×9 grid and colorized using the jet colormap (Glu) and hot colormap (NAA). This 9×9 grid was then over layed onto an anatomical grayscale image for the entire FOV. For CSI difference spectrum, exponential line broadening (3 Hz) was applied to each individual spectrum, and the post infusion spectrum was automatically shifted, phase corrected, and Voigt lineshape filtered to minimize differences between the pre- and post-infusion spectrum over the spectral ranges where no changes occurred.

Quantification of DMRS data was performed with the jMRUI software package (Version 6.0) using a non-linear least-squares quantitation algorithm named Advanced Method for Accurate, Robust and Efficient Spectral (AMARES) fitting[23] by normalizing metabolite

levels to the natural abundance deuterated water signal. As some deuterium labelling of water will occur following infusion of deuterated glucose, we normalized metabolite concentrations to the ratio of post-infusion water levels at each timepoint to pre-infusion levels. SNR estimates were calculated by taking the peak area and dividing it by the standard deviation of the noise level in the spectrum.

Data presentation

All statistical analyses and graphical display of datasets was performed using GraphPad Prism (Version 7.0) for MacOS (GraphPad Software, La Jolla, CA). Minor smoothing was applied to difference spectra plots using a 2^{nd}-order polynomial averaging three neighboring points on each side. All LCModel derived metabolite concentration plots report mean values with standard error of the mean. Fitted curves for concentration plots were generated to provide a visual aid of labelling using the following exponential plateau equation, $Y=Y_M - (Y_M-Y_0)*\exp(-k*x)$, where Y_0 is the starting population, Y_M is the maximum population, and K is the rate constant. Pearson's correlation analysis and Bland-Altman analysis was performed to compare Glx measurements made with qMRS and DMRS. $P<0.05$ was considered significant.

Reporting Summary

Further information on research design is available in the Nature Research Reporting Summary linked to this article.

Data availability

The main data supporting the results in this study are available within the paper and its Supplementary Information. The raw and analysed datasets generated during the study are too big to be publicly shared, yet they are available for research purposes from the corresponding authors on reasonable request.

Supplementary Material

Refer to Web version on PubMed Central for supplementary material.

Acknowledgements

The authors would thank Dr. Damodara Reddy for help with animal model preparation, Dr. Mark Elliot for his expertise on MRS acquisition and processing, and Drs. Stephen Pickup and Weixia Liu for their technical assistance in using the 9.4 T horizontal bore animal MR scanner. The authors would especially like to thank Gabor Mizsei for constructing the deuterium coil, Dr. Harish Poptani for providing insight into CSI acquisition and processing on the 9.4T preclinical scanner, and Dr. Robin de Graaf for providing guidance during interfacing of the deuterium coil to the scanner console. This work was carried out at a US National Institutes of Health-supported resource, with funding from: the NIBIB under Grant No. P41 EB015893, National Institute of Neurological Disorders and Stroke Award Number R01NS087516 and the training grant T32EB020087-02.

References

1. DeBerardinis RJ & Thompson CB Cellular metabolism and disease: what do metabolic outliers teach us? Cell. 148, 1132–1144 (2012). [PubMed: 22424225]

2. Pavlova NN & Thompson CB The Emerging Hallmarks of Cancer Metabolism. Cell Metab. 23, 27–47 (2016). [PubMed: 26771115]
3. Fuss TL & Cheng LL Metabolic Imaging in Humans. Top. Magn. Reson. Imaging 25, 223–235 (2016). [PubMed: 27748708]
4. Kelloff GJ et al. Progress and promise of FDG-PET imaging for cancer patient management and oncologic drug development. Clin. Cancer Res. 11, 2785–2808 (2005) [PubMed: 15837727]
5. Duara R et al. Positron emission tomography in Alzheimer's disease. Neurology 36, 879–87 (1986) [PubMed: 3487046]
6. Bergquist PJ et al. Cardiac Applications of PET-MR. Curr. Cardiol. Rep 19, 42 (2017) [PubMed: 28401505]
7. la Fougere C, Suchorska B, Bartenstein P, Kreth FW, & Tonn JC Molecular imaging of gliomas with PET: opportunities and limitations. Neuro. Oncol 13, 806–819 (2011) [PubMed: 21757446]
8. Morris PG Nuclear magnetic resonance imaging in medicine and biology. (Clarendon Press, 1986).
9. Van Zijl PC, & Yadav NN Chemical exchange saturation transfer (CEST): what is in a name and what isn't?. Magn. Reson. Med, 65, 927–948. (2011) [PubMed: 21337419]
10. Cai K et al. Magnetic resonance imaging of glutamate. Nat. Med 18, 302 (2012) [PubMed: 22270722]
11. Gujar SK, Maheshwari S, Björkman-Burtscher I & Sundgren PC Magnetic resonance spectroscopy. J. Neuroophthalmol 25, 217–26 (2005) [PubMed: 16148633]
12. Beckmann N, Turkalj I, Seelig J, & Keller U Carbon-13 NMR for the assessment of human brain glucose metabolism in vivo. Biochemistry, 30, 6362–6366 (1991) [PubMed: 2054342]
13. Shulman RG & Rothman DL ^{13}C NMR of Intermediary Metabolism: Implications for Systemic Physiology. Annu. Rev. Physiol 63, 15–48 (2001) [PubMed: 11181947]
14. de Graaf RA, Rothman DL, & Behar KL State of the art direct 13C and indirect 1H-[13C] NMR spectroscopy in vivo. A practical guide. NMR Biomed, 24, 958–972 (2011) [PubMed: 21919099]
15. Merritt ME, Harrison C, Storey C, Jeffrey FM, Sherry AD, & Malloy CR Hyperpolarized 13C allows a direct measure of flux through a single enzyme-catalyzed step by NMR. Proc. Natl. Acad. Sci 104, 19773–19777 (2007) [PubMed: 18056642]
16. Ross BD, Bhattacharya P, Wagner S, Tran T & Sailasuta N Hyperpolarized MR imaging: Neurologic applications of hyperpolarized metabolism. Am. J. Neuroradiol 31, 24–33 (2010) [PubMed: 19875468]
17. Lu M, Zhu XH, Zhang Y, Mateescu G & Chen W Quantitative assessment of brain glucose metabolic rates using in vivo deuterium magnetic resonance spectroscopy. J. Cereb. Blood Flow Metab. 37, 3518–3530 (2017) [PubMed: 28503999]
18. De Feyter HM et al. Deuterium metabolic imaging (DMI) for MRI-based 3D mapping of metabolism in vivo. Sci. Adv 4, eaat7314 (2018) [PubMed: 30140744]
19. Zhang L et al. Spectral tracing of deuterium for imaging glucose metabolism. Nat. Biomed. Eng 3, 402–413 (2019) [PubMed: 31036888]
20. Brindle KM Imaging Metabolism with Hyperpolarized ^{13}C-Labelled Cell Substrates. J. Am. Chem. Soc 20, 6418–6427 (2015)
21. De Graaf RA, Mason GF, Patel AB, Behar KL & Rothman DL In vivo 1H-[13C]-NMR spectroscopy of cerebral metabolism. NMR Biomed. 16, 339–357 (2003) [PubMed: 14679499]
22. Provencher SW Estimation of metabolite concentrations from localized in vivo proton NMR spectra. Magn. Reson. Med 30, 672–679 (1993) [PubMed: 8139448]
23. Naressi A, Couturier C, Castang I, de Beer R & Graveron-Demilly D Java-based graphical user interface for MRUI, a software package for quantitation of in vivo/medical magnetic resonance spectroscopy signals. Comput. Biol. Med 31, 269–286 (2001) [PubMed: 11334636]
24. Van Eijsden P, Behar KL, Mason GF, Braun KP, & De Graaf RA In vivo neurochemical profiling of rat brain by ^{1}H-[^{13}C] NMR spectroscopy: cerebral energetics and glutamatergic/GABAergic neurotransmission. J. Neurochem 112, 24–33 (2010) [PubMed: 19818103]
25. Baslow MH N-acetylaspartate in the vertebrate brain: Metabolism and function. Neurochem. Res 28, 941–953 (2003) [PubMed: 12718449]

26. Heiden M. G.VanderCantley LC &Thompson CB Understanding the warburg effect: The metabolic requirements of cell proliferation. Science. 324, 1029–1033 (2009) [PubMed: 19460998]
27. Wilson M, et al. Methodological consensus on clinical proton MRS of the brain: Review and recommendations. Magn. Reson. Med 82, 527–550 (2019) [PubMed: 30919510]
28. Donoho DL De-noising by soft-thresholding. IEEE T. Inform. Theory 41, 613–627 (1995).
29. Johnstone IM, & Silverman BW (2004). Needles and straw in haystacks: Empirical Bayes estimates of possibly sparse sequences. The Annals of Statistics, 32(4), 1594–1649.
30. Brender JR et al. Dynamic Imaging of Glucose and Lactate Metabolism by 13C-MRS without Hyperpolarization. Sci. Rep 9, 3410 (2019) [PubMed: 30833588]
31. Mason GF et al. Simultaneous Determination of the Rates of the TCA Cycle, Glucose Utilization, α-Ketoglutarate/Glutamate Exchange, and Glutamine Synthesis in Human Brain by NMR. J. Cereb. Blood Flow Metab. 15, 12–25 (1995) [PubMed: 7798329]
32. Bak LK, Schousboe A & Waagepetersen HS The glutamate/GABA-glutamine cycle: Aspects of transport, neurotransmitter homeostasis and ammonia transfer. J. Neurochem 98, 641–653 (2006) [PubMed: 16787421]
33. Wong CGT, Bottiglieri T & Snead OC GABA, γ-hydroxybutyric acid, and neurological disease. Ann. Neurol 54, S3–S12 (2003)
34. Rothman DL, de Graaf RA, Hyder F, Mason GF, Behar KL, & De Feyter HM In vivo 13C and 1H-[13C] MRS studies of neuroenergetics and neurotransmitter cycling, applications to neurological and psychiatric disease and brain cancer. NMR Biomed. e4172 (2019) [PubMed: 31478594]
35. Shulman RG, & Rothman DL ^{13}C NMR of intermediary metabolism: implications for systemic physiology. Ann. Rev. Phys 63, 15–48 (2001)
36. Henry PG, et al. In vivo 13C NMR spectroscopy and metabolic modeling in the brain: a practical perspective. Magn. Reson. Imaging, 24, 527–539 (2006) [PubMed: 16677959]
37. Tiwari V, Ambadipudi S, & Patel AB Glutamatergic and GABAergic TCA cycle and neurotransmitter cycling fluxes in different regions of mouse brain. J. Cereb. Blood Flow Metab. 33, 1523–1531 (2013) [PubMed: 23838829]
38. Duarte JM, & Gruetter R Glutamatergic and GABAergic energy metabolism measured in the rat brain by 13C NMR spectroscopy at 14.1 T. J. Neurochem 126, 579–590 (2013) [PubMed: 23745684]
39. Kreis R Issues of spectral quality in clinical 1H-magnetic resonance spectroscopy and a gallery of artifacts. NMR Biomed, 17, 361–381 (2004) [PubMed: 15468083]
40. Mullins PG, Chen H, Xu J, Caprihan A, & Gasparovic C Comparative reliability of proton spectroscopy techniques designed to improve detection of J-coupled metabolites. Magn. Reson. Med, 60, 964–969 (2008) [PubMed: 18816817]
41. Trabesinger AH, Weber OM, Duc CO, & Boesiger P Detection of glutathione in the human brain in vivo by means of double quantum coherence filtering. Magn. Reson. Med 42, 283–289 (1999) [PubMed: 10440953]
42. Ko L, Koestner A, & Wechsler W Morphological characterization of nitrosourea-induced glioma cell lines and clones. Acta neuropathol, 51, 23–31 (1980) [PubMed: 7435138]
43. Kim S, Pickup S, Hsu O & Poptani H Diffusion tensor MRI in rat models of invasive and well-demarcated brain tumors. NMR Biomed. 21, 208–216 (2008) [PubMed: 17530617]
44. Fitzpatrick SM, Hetherington HP, Behar KL & Shulman RG The flux from glucose to glutamate in the rat brain in vivo as determined by ^{1}H-observed, ^{13}C-edited NMR spectroscopy. J. Cereb. Blood Flow Metab. 10, 170–179 (1990) [PubMed: 1968068]
45. Patlak CS, & Pettigrew KD A method to obtain infusion schedules for prescribed blood concentration time courses. J. Appl. Physiol 40, 458–463 (1976) [PubMed: 819414]
46. Bottomley PA Spatial localization in NMR spectroscopy in vivo. Ann. N.Y. Acad. Sci 508, 333–348 (1987) [PubMed: 3326459]
47. Tkáč I, Starčuk Z, Choi IY, & Gruetter R In vivo 1H NMR spectroscopy of rat brain at 1 ms echo time. Magn. Reson. Med 41, 649–656 (1999) [PubMed: 10332839]

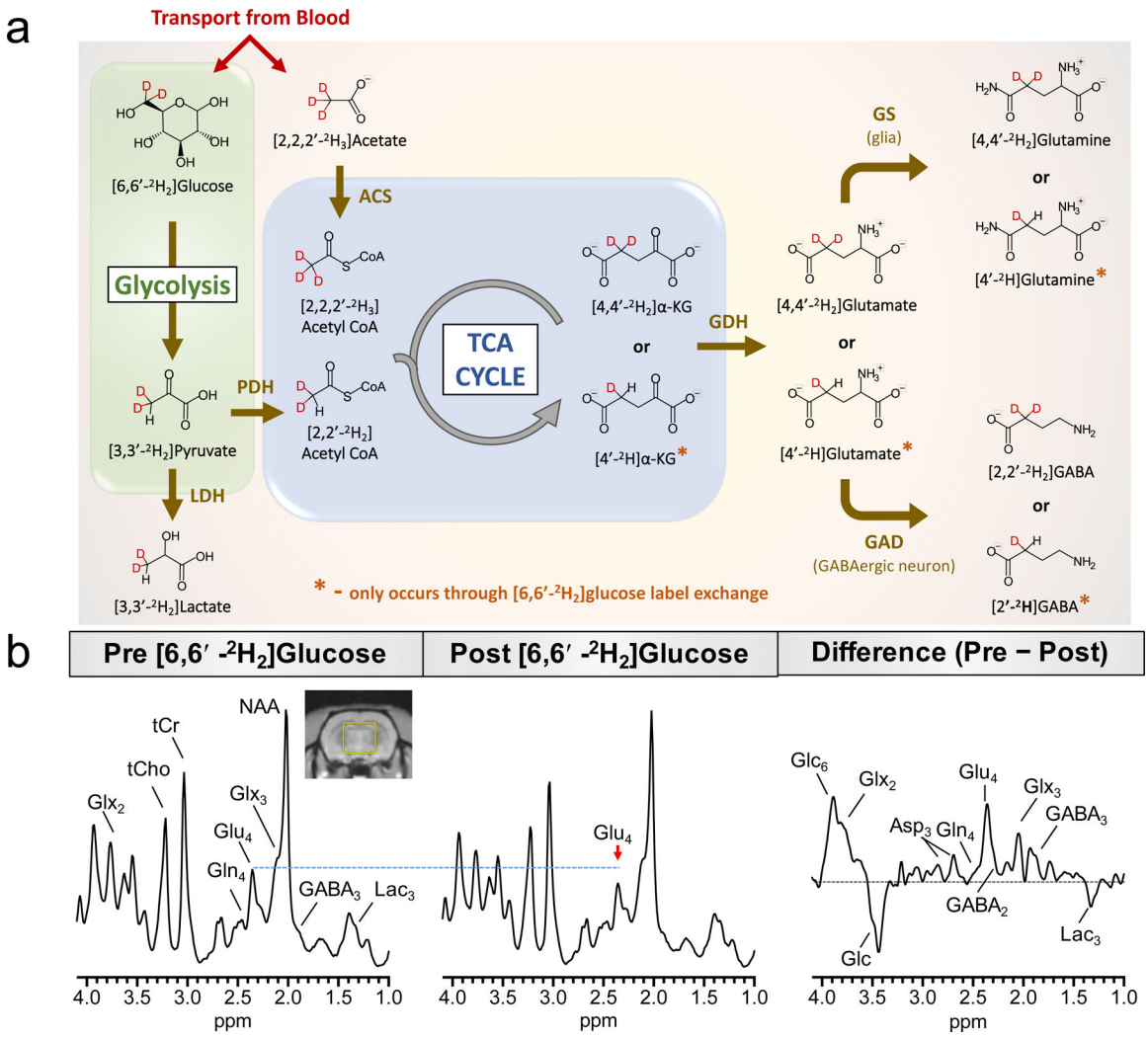

Figure 1. Fundamentals of qMRS.

a, Schematic shows pathway, including important enzymes, for exchange of deuterium from [6,6′−$^{2}H_2$]glucose and [2,2,2′−$^{2}H_3$]acetate to downstream metabolites that can be detected with ^{1}H MRS. **b**, Displayed ^{1}H MRS spectra (10 min acquisition, 256 averages) acquired before and after 60 minutes of [6,6′−$^{2}H_2$]glucose infusion shows decrease in Glu-H4 (Glu_4, blue line). Spectra were obtained from the midbrain region as shown in the representative anatomical image (yellow outline). qMRS difference spectra shows clear labelling of Glu_4, in addition to several Gln GABA, Glucose (Glc) and Asp resonances. Asp aspartate, ACS acetyl coA synthetase, GABA γ-aminobutyric acid, GAD glutamate decarboxylase, GDH glutamate dehydrogenase, Glc glucose, Glu glutamate, Gln glutamine, Glx Glu+Gln, GS glutamine synthetase, α-KG α-ketoglutarate, Lac lactate, LDH lactate dehydrogenase, NAA N-acetyl aspartate, PDH pyruvate dehydrogenase, tCr total creatine, tCho total choline

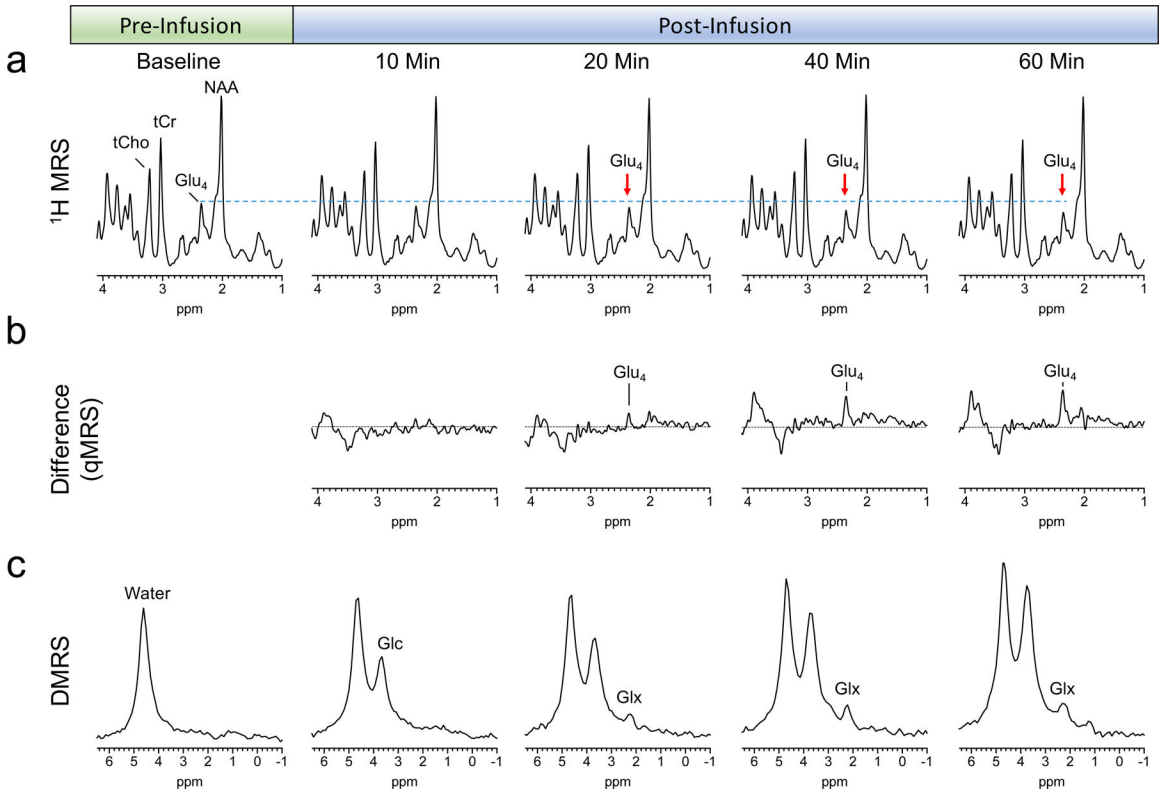

Figure 2. Simultaneous qMRS and DMRS acquisition in normal rat brain.

a, Displayed ^{1}H MR spectra (10 min acquisition, 256 averages) show continuous reduction in 2.35 ppm Glu-H4 peak (Glu_4, red arrow) following infusion of [6,6′−$^{2}H_2$]glucose. **b**, qMRS difference spectra show gradual accumulation of ^{2}H labelled Glu-H4 beginning after 20 mins of infusion. **c**, Similarly, DMRS spectra (5 min acquisition, 1000 averages) also revealed a gradual increase in Glx peak observed beginning 20 min after infusion. Glu glutamate, Glx Glu+Gln, Lac lactate, NAA N-acetyl aspartate, tCr total creatine, tCho total choline

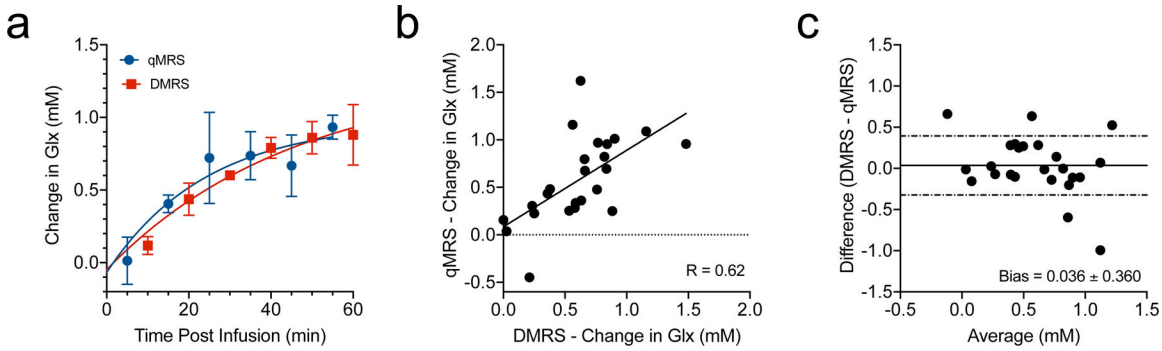

Figure 3. Comparison of qMRS and DMRS metabolite quantification.

a, Graph shows changes in Glx concentration in normal rat brain (n=4) measured with qMRS (blue) and DMRS (red) made during [6,6′−$^{2}H_{2}$]glucose infusion. For a visual aid, concentration estimates were fitted with the exponential plateau equation $Y=Y_M-(Y_M-Y_0)*\exp(-k*x)$, where Y_0 is the starting population, Y_M is the maximum population, and k is the rate constant. **b**, Correlation plot with Pearson's correlation analysis shows relationship between these quantitative measurements at each time point post infusion. **c**, Bland-Altman plot and bias analysis showing the mean bias (solid line) and standard deviation (dashed lines) for Glx measurements made with qMRS and DMRS. Error bars represent the standard error of the mean.

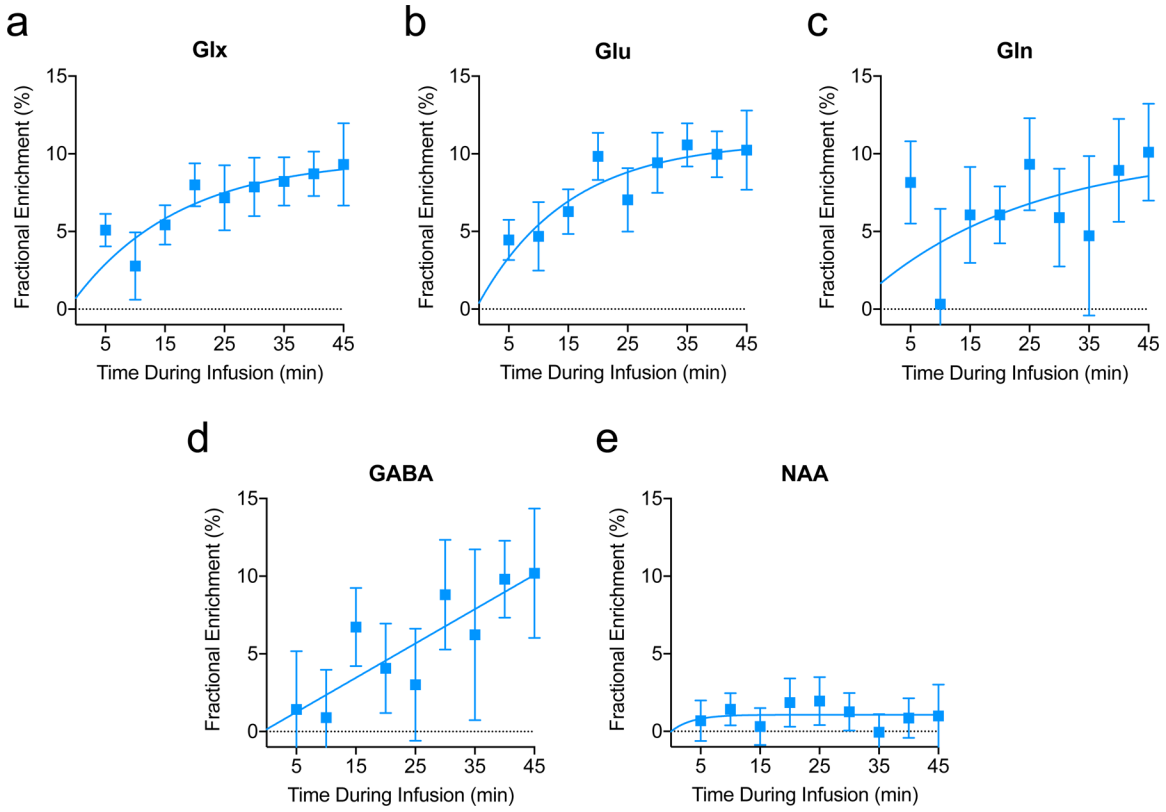

Figure 4. Kinetics of deuterium labelling of neural metabolites.

Graphs show fractional enrichment for (**a**) Glx, (**b**) Glu, (**c**) Gln, (**d**) GABA, and (**e**) NAA measured in normal rat brain (n=6) during [6,6′−$^{2}H_{2}$]glucose infusion acquired over a 45 min period. For a visual aid, plots were fitted with the exponential plateau equation $Y=Y_M - (Y_M-Y_0)*\exp(-k*x)$, where Y_0 is the starting population, Y_M is the maximum population, and k is the rate constant. Error bars represent the standard error of the mean.

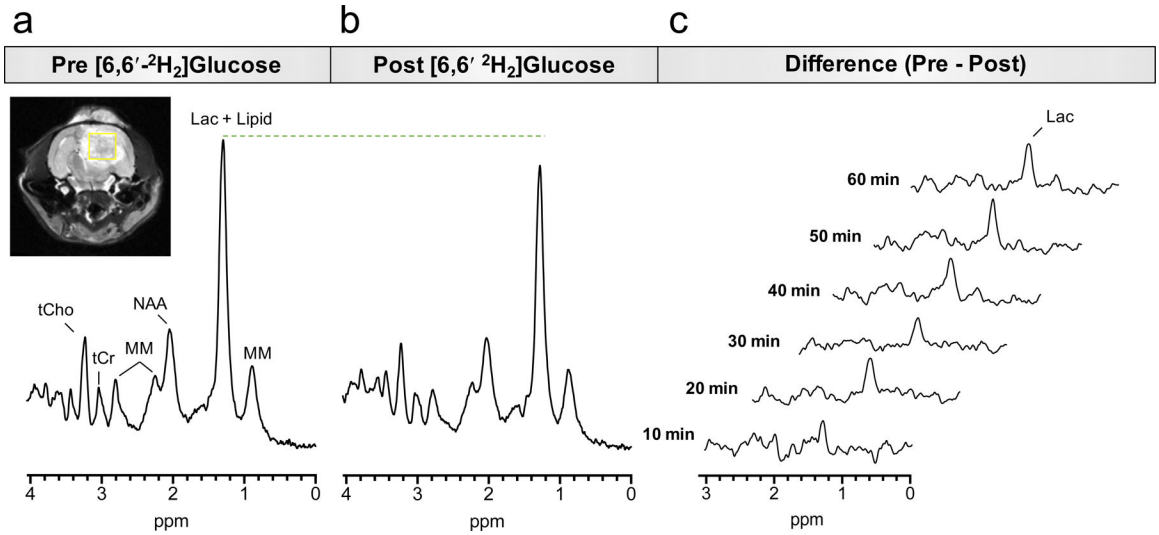

Figure 5. Detection of glycolysis in rat glioblastoma.

Studies were performed in rats (n=3) bearing orthotopic F98 glioblastoma. **a**, Obtained spectrum (5 min acquisition, 128 averages) show a large lac/lipid peak observed at 1.33 ppm from a voxel placed within the tumour (inset). **b**, Spectrum acquired after 60 minutes of [6,6′−$^{2}H_2$]glucose infusion shows a marked reduction in the 1.33 peak (green line). **c**, qMRS difference spectra (pre-post) obtained every 10 minutes post infusion show the increase in labelled lac at 1.33 ppm. Lac lactate, MM macromolecules, NAA N-acetyl aspartate, tCr total creatine, tCho total choline

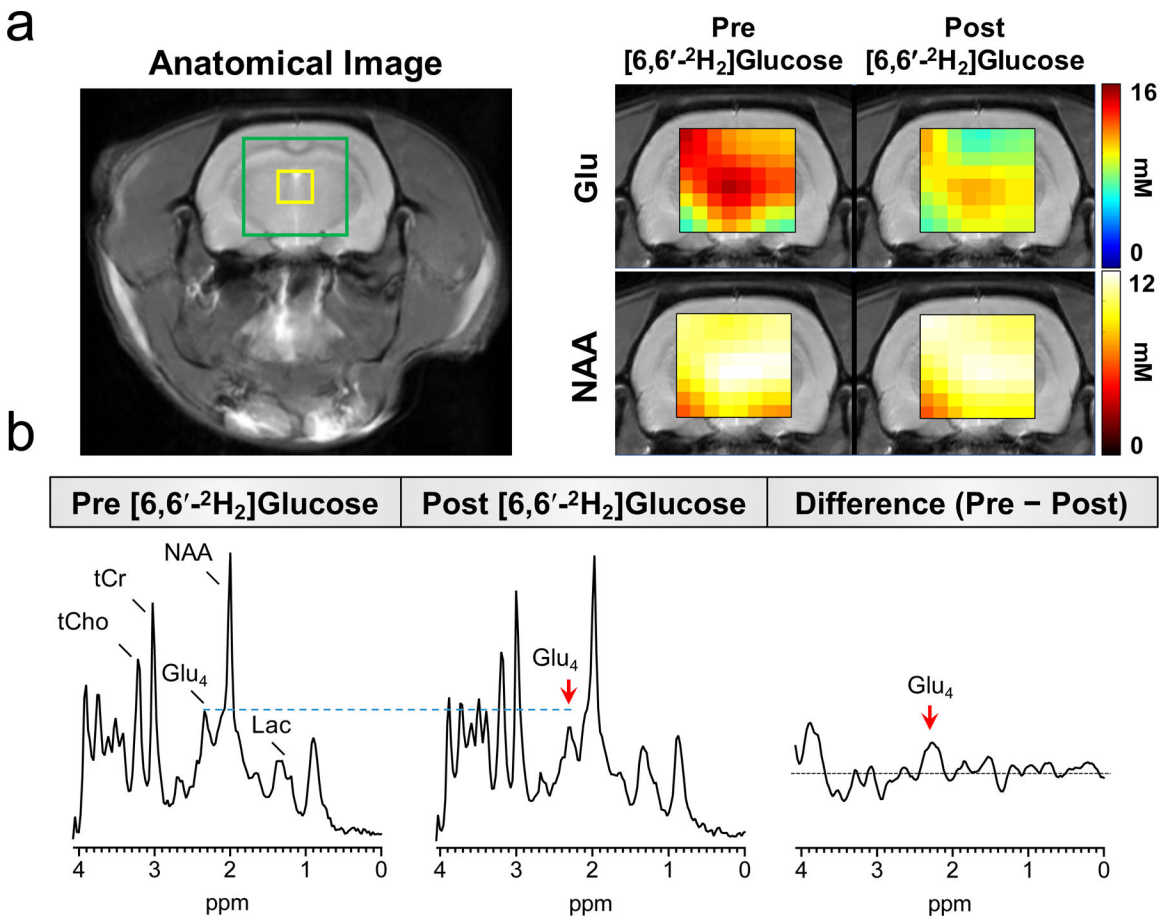

Figure 6. Metabolic imaging of neural metabolism.

a, Images show anatomical reference image (left) with sampled volume of interest (VOI, green box) for Chemical Shift Imaging and corresponding Glu and NAA metabolite maps (right) acquired in a normal rat brain at 9.4T before and after 60 min of [6,6′−$^{2}H_2$]glucose infusion. **b**, Displayed spectra represent a single CSI voxel within the VOI (yellow box) acquired before and after infusion. A clear reduction in Glu-H4 resonance (Glu_4) can be observed post infusion (red arrow). Glu_4 peak was also observed in the corresponding difference spectrum. Glu glutamate, Glx glu-gln, Lac lactate, NAA N-acetyl aspartate, tCr total creatine, tCho total choline